ORIGINAL ARTICLE OPEN ACCESS

Identification and Characterization of Innate Immunity in *Actinidia melanandra* in Response to *Pseudomonas syringae* pv. actinidiae

Lauren M. Hemara[1,2] | Abhishek Chatterjee[2] | Shin-Mei Yeh[2] | Ronan K. Y. Chen[3] | Elena Hilario[2] | Liam Le Lievre[2,4] | Ross N. Crowhurst[2] | Deborah Bohne[2] | Saadiah Arshed[2] | Haileigh R. Patterson[1,2] | Kelvina Barrett-Manako[2] | Susan Thomson[5] | Andrew C. Allan[2] | Cyril Brendolise[2] | David Chagné[3] | Matthew D. Templeton[1,2] | Jibran Tahir[2] | Jay Jayaraman[2]

[1]School of Biological Sciences, The University of Auckland, Auckland, New Zealand | [2]The New Zealand Institute for Plant and Food Research Limited, Mount Albert Research Centre, New Zealand | [3]The New Zealand Institute for Plant and Food Research Limited, Palmerston North, New Zealand | [4]Department of Biochemistry, University of Otago, Dunedin, New Zealand | [5]The New Zealand Institute for Plant and Food Research Limited, Lincoln Research Centre, New Zealand

Correspondence: Jibran Tahir (jibran.tahir@hill-labs.co.nz) | Jay Jayaraman (Jay.Jayaraman@plantandfood.co.nz)

ABSTRACT

Pseudomonas syringae pv. *actinidiae* biovar 3 (Psa3) has decimated kiwifruit orchards growing susceptible kiwifruit *Actinidia chinensis* varieties. Effector loss has occurred recently in Psa3 isolates from resistant kiwifruit germplasm, resulting in strains capable of partially overcoming resistance present in kiwiberry vines (*Actinidia arguta*, *Actinidia polygama*, and *Actinidia melanandra*). Diploid male *A. melanandra* recognises several effectors, sharing recognition of at least one avirulence effector (HopAW1a) with previously studied tetraploid kiwiberry vines. Sequencing and assembly of the *A. melanandra* genome enabled the characterisation of the transcriptomic response of this non-host to wild-type and genetic mutants of Psa3. *A. melanandra* appears to mount a classic effector-triggered immunity (ETI) response to wildtype Psa3 V-13, as expected. Surprisingly, the type III secretion (T3SS) system-lacking Psa3 V-13 Δ*hrcC* strain did not appear to trigger pattern-triggered immunity (PTI) despite lacking the ability to deliver immunity-suppressing effectors. Contrasting the *A. melanandra* responses to an effectorless Psa3 V-13 Δ*33E* strain and to Psa3 V-13 Δ*hrcC* suggested that PTI triggered by Psa3 V-13 was based on the recognition of the T3SS itself. The characterisation of both ETI and PTI branches of innate immunity responses within *A. melanandra* further enables breeding for durable resistance in future kiwifruit cultivars.

1 | Introduction

Kiwifruit (*Actinidia* spp.) is a valuable perennial crop threatened by the bacterial pathogen *Pseudomonas syringae* pv. *actinidiae* (Psa) (Mauri et al. 2016; McCann et al. 2017; Donati et al. 2020; Scortichini, Spinelli and Templeton 2023). Psa biovar 3 (Psa3) spread throughout kiwifruit-growing regions worldwide during a pandemic in the late 2000s, causing significant economic losses. In New Zealand, Psa3 V-13 (ICMP 18884) represents the initial Psa3 incursion that decimated orchards growing a monoculture of the highly susceptible cultivar *Actinidia chinensis* var. *chinensis* 'Hort16A' (Vanneste 2017). Replacing 'Hort16A' with less susceptible cultivars has helped the New Zealand kiwifruit industry recover from the

impact of this disease since the initial incursion. However, Psa remains a persistent challenge, requiring significant time and expense to control through chemical applications and orchard hygiene practices. The use of copper-based sprays was effective in managing Psa, but copper use is considered dangerous and its use in several countries is restricted or being phased out. In addition, use of copper has led to the wide-spread emergence of copper-tolerant Psa3 strains through the acquisition of copper resistance genes on integrative conjugative elements and plasmids, increasing Psa's copper minimum inhibitory concentration up to and over 1.6 mM $CuSO_4$ with the formation of pathogen consortia to overcome copper resistance also observed (Colombi et al. 2017; Petriccione et al. 2017; Aono et al. 2024). While this has not eliminated copper use efficacy yet, to sustainably manage Psa long-term, there is a need to diversify Psa management strategies and develop durable Psa-resistant kiwifruit cultivars.

To breed durable pathogen resistance in crops, it is important to capture the causal genetic loci for diverse modes of plant immunity. Previously, it was shown within the commercially dominant *A. chinensis* species complex that Psa tolerance and susceptibility are mostly associated with multiple loci in yellow-fleshed tetraploid and diploid outcrosses in field conditions (Tahir et al. 2019, 2020). Some degree of Psa resistance has been observed within the *A. chinensis* species complex. Surveys suggest that other *Actinidia* species in the Leiocarpae section (colloquially termed kiwiberry), including *Actinidia macrosperma*, *Actinidia valvata*, *Actinidia polygama*, *Actinidia hypoleuca*, *Actinidia arguta* and *Actinidia melanandra* could potentially be Psa-resistant, with fewer vines removed from the Te Puke Research Orchard germplasm collection in New Zealand because of Psa infection (Datson et al. 2015). These potentially Psa-resistant species also fall clearly within the monophyletic smooth-skinned fruit clade (Liu et al. 2017). *A. melanandra* is native to the Hubei and Yunnan provinces of China, has purple-red kiwiberry fruit, and is of particular interest owing to several diploid genotypes being identified (Datson et al. 2015). Psa3 symptoms have previously been observed on a commercial *A. arguta* orchard; however, both the appearance of symptoms and the impact on orchard production were very limited (Vanneste et al. 2014). Inter-specific hybridisation in kiwifruit will open doors to more robust genetic combinations against the more rapidly evolving pathogen (Z. Wang et al. 2017).

Plant innate immunity is a complex process that consists of two interconnected layers, namely pattern-triggered immunity (PTI) and effector-triggered immunity (ETI). PTI is triggered by the recognition of highly conserved pathogen-associated molecular patterns at the host cell membrane. ETI is a more specific response that is activated by the presence or activity of one or more pathogen effector proteins, typically within the host cell. ETI potentiates and amplifies PTI, often culminating in a hypersensitive response, leading to the death of infected cells to protect the rest of the plant (Ngou et al. 2021; Yuan et al. 2021). While ETI can be highly effective in protecting plants from disease, resistance mediated by a single resistance (R) gene may be vulnerable to resistance breakdown because of pathogen evolution. R gene stacking may increase the durability of resistance in the field by providing multiple avenues of pathogen recognition that are harder for the pathogen to evade.

In Psa-resistant kiwiberry *A. arguta* versus Psa-susceptible *A. chinensis*, ETI and PTI responses can be affected by the presence or absence of avirulence and virulence Psa effectors (Hemara et al. 2022; Jayaraman et al. 2021, 2023). The molecular signatures underlying these dynamically interconnected modes of host immunity can help identify pathways that are specifically activated and co-evolved in both compatible and incompatible kiwifruit-Psa interactions. In this current study, the emergence of Psa3 effector-variant strains on various host kiwifruit species was explored and a diploid kiwiberry model system (*A. melanandra*) was utilised to dissect layers of innate immune response to Psa3. By exploring the transcriptional landscape to infiltration by virulent and non-virulent strains of Psa3 and *Pseudomonas fluorescens* (Pfo) in the diploid Psa3-resistant *A. melanandra*, ETI and PTI pathways in *Actinidia* were characterised. This will allow for the mapping of novel genes for resistance and breeding cultivars that will have durable, long-term resistance to Psa in the orchard.

2 | Results

2.1 | Psa3 Lineages With Deleted Effectors Have Emerged Independently and Multiple Times on Psa-Resistant *Actinidia* Vines

hopAW1a loss has been previously reported on *A. arguta*, as typified by Psa3 X-27 (Hemara et al. 2022). Following Psa3 genome bio-surveillance in the *Actinidia* germplasm collection at Te Puke, New Zealand, from 2017 to 2022, the further independent emergence of two additional lineages with deletions in the exchangeable effector locus (EEL) was observed (Figure 1A). Most EEL-loss isolates have a 51 kb deletion mediated by recombination at DD[E/D] transposases (DDEs) and Miniature inverted-repeat transposable elements (MITEs). However, Psa3 X-469 has a smaller 38 kb deletion, which removes *hopQ1a*, *hopD1a*, *avrD1*, *avrB2b*, *hopAB1ak* and *hopF4a* alongside *hopAW1a*, *hopF1e*, *hopAF1b*, *hopD2a* and *hopF1a* (Figures 1A and S1A). Unlike Psa3 X-27, Psa3 X-469 retains the non-ribosomal peptide synthetase (NRPS) toxin biosynthesis cluster. This deletion appears to be mediated by recombination at the flanking MITEg3 and MITEg8 elements (Figure S1A). The emergence of two independent *avrRpm1a* loss lineages was also observed (Figure 1A). The *avrRpm1a* deletion of 11 kb is flanked by Tn family 21 and DDEg14 (Figure S1B). Both *hopAW1a* and *avrRpm1a* are known to be recognised by Psa-resistant *A. arguta* (Hemara et al. 2022). Interestingly, the loss of *hopZ5a* or *hopF1c* from isolates collected from these diverse germplasm vines was never observed. This is despite the fact that *hopZ5a* (like *avrRpm1a* that is lost from the orchard isolates) is recognized by *A. arguta* and is 'cargo' on an exapt ICE-A, a remnant, non-mobile integrative conjugative element that lacks a t-RNA-Lys attachment (att) site for excision (Hemara et al. 2022; Poulter et al. 2018). In summary, several isolates have been recovered from newly symptomatic material from Psa-resistant *Actinidia* germplasm. Several of these isolates showed signs of effector loss that may be related to effector recognition by the vines these isolates were sampled from. These findings hint at the possibility that the emergence of symptoms is associated with effector loss and the involvement of ETI in resistance to Psa in these vines.
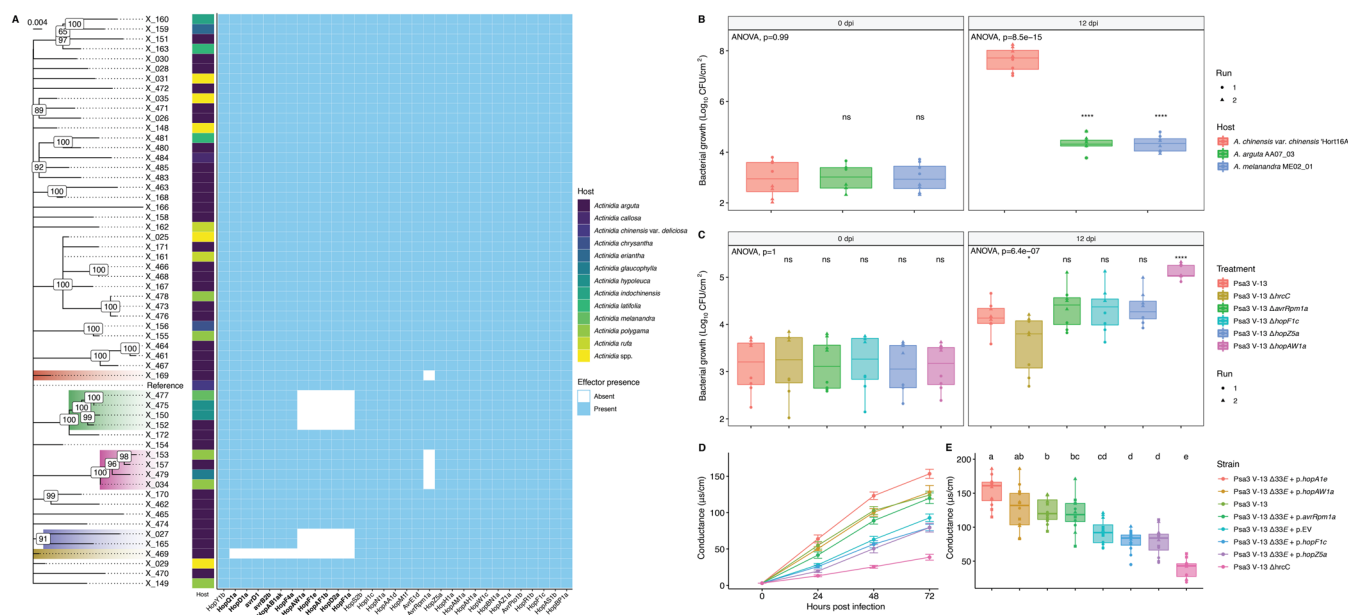
FIGURE 1 | *Actinidia melanandra* mounts an effector-triggered defence response against *Pseudomonas syringae* pv. *actinidiae* (Psa3) V-13. (A) Core SNP phylogeny of Psa isolates from germplasm *Actinidia* vines. Effector presence and absence by genome position indicate the emergence of multiple lineages of exchangeable effector locus (EEL) and *avrRpm1a* loss variants. Effectors in the EEL are highlighted in bold. (B) *A. chinensis* var. *chinensis* 'Hort16A', *Actinidia arguta* AA07_03, and *A. melanandra* ME02_01 plantlets were flood-inoculated with Psa3 V-13 at approximately 10^6 CFU/mL. Bacterial growth was quantified relative to 'Hort16A' at 0 and 12 days postinoculation by plate count. Box and whisker plots, with black bars representing the median values for the four pseudobiological replicates and whiskers representing the 1.5 interquartile range. Asterisks indicate the statistically significant difference of Student's *t*-test between the indicated species and *A. chinensis* var. *chinensis* 'Hort16A', where *$p \leq 0.05$, **$p \leq 0.01$, ***$p \leq 0.001$ and $^{ns}p > 0.05$ (not significant). (C) *A. melanandra* ME02_01 plantlets were flood-inoculated with Psa3 V-13 effector knockout strains at approximately 10^6 CFU/mL. Bacterial growth was quantified relative to Psa3 V-13 at 0 and 12 days postinoculation by plate count. Box and whisker plots, with black bars representing the median values for the four pseudobiological replicates and whiskers representing the 1.5 interquartile range. Asterisks indicate the statistically significant difference of Student's *t*-test between the indicated strain and wild-type Psa3 V-13, where *$p \leq 0.05$, **$p \leq 0.01$, ***$p \leq 0.001$ and $^{ns}p > 0.05$ (not significant). (D, E) Leaf discs from *A. melanandra* ME02_01 plantlets were vacuum-infiltrated with Psa3 V-13 or Psa3 V-13 Δ33E carrying empty vector (EV) or a plasmid-borne type III secreted effector (*hopAW1a*, *hopZ5a*, *avrRpm1a* or *hopF1c*, or positive control *hopA1j* from *P. syringae* pv. *syringae* 61) inoculum at ~5×10^8 CFU/mL. (D) Electrical conductivity due to HR-associated ion leakage was measured at indicated times over 72 h. The ion leakage curves are stacked for three independent runs of this experiment. Error bars represent the standard errors of the means calculated from the five pseudobiological replicates per experiment ($n = 15$). (E) Tukey's HSD with different letters indicates treatment groups that are significantly different at the 72-h timepoint ($\alpha \leq 0.05$). [Color figure can be viewed at wileyonlinelibrary.com]

While the majority of these effector-loss strains have been isolated from *A. arguta*, EEL loss isolates have also been found on *A. hypoleuca* and *A. melanandra* vines, and *avrRpm1a* loss isolates have been found on *A. polygama* and *A. glaucophylla* (Figure 1A). *A. melanandra* is a species of interest because diploid members of this species possess resistance against Psa3, and its simple ploidy makes it amenable to genome sequencing and a less complex genome assembly, and utility in mapping target loci for breeding.

2.2 | *A. melanandra* Recognises HopAW1a, HopBP1a and AvrRpm1a

A. melanandra (accession ME02_01) restricts the bacterial growth of wild-type Psa3 V-13, similarly to *A. arguta*, suggesting that *A. melanandra* might also recognise Psa3 through ETI (Figure 1B). DAB staining indicates the production of reactive oxygen species (ROS) in the presence of Psa3 V-13, but not Psa3 V-13 Δ*hrcC*, supporting the existence of ETI in this accession (Figure S2). However, *A. melanandra* may not necessarily

recognise the same effector profile that *A. arguta* does. When comparing knockout strains for the four effectors recognized by *A. arguta*, only Psa3 Δ*hopAW1a* grew better than wild-type Psa3 on *A. melanandra*, while Δ*avrRpm1a*, Δ*hopF1c* and Δ*hopZ5a* strains were not significantly different from wild-type Psa3 (Figure 1C). To observe ETI-associated ion leakage, *P. fluorescens* carrying a T3SS from *P. syringae* pv. *syringae* 61 (Pfo (T3SS); Thomas et al. 2009), was used to deliver individual Psa3 V-13 effectors into *A. melanandra* (Figure S3). Only HopAW1a and HopBP1a (both weakly) triggered ion leakage in ME02_01, suggesting some effector recognition (Figure S3). This result was confirmed by a reporter eclipse assay (Jayaraman et al. 2021), demonstrating that both HopAW1a and HopBP1a, like the avirulence effector control HopA1j from *P. syringae* pv *syringae* 61, are recognized in *A. melanandra* (Figure S4).

Pfo(T3SS) may not be able to express and deliver effectors from Psa in the full context of a suite of other potential pathogenicity factors. To mimic this more complete context and deliver individual effectors from Psa3, a complete effector knockout strain (Psa3 V-13 Δ*33E*) was generated that lacked all 33

expressed effectors. To confirm that the AA07_03-recognized avirulence effectors were not affected by their level of expression under the synthetic promoter or the C-terminal HA tag, *hopAW1a*, *hopZ5a*, *avrRpm1a* and *hopF1c* (with *shcF* carrying a point mutation resulting in an early truncation) were cloned under their native promoters. Psa3 V-13 Δ*33E* delivery of HopAW1a, HopZ5a, AvrRpm1a and HopF1c revealed that HopAW1a and AvrRpm1a were able to trigger ion leakage in ME02_01 leaves, confirming resistance in *A. melanandra* ME02_01 is due to ETI (Figure 1D,E). Curiously, Psa3 Δ*33E* + EV also appeared to trigger some ion leakage, despite lacking any functional effectors from Psa3 (Figure 1D,E). This was not the case for Psa3 V-13 Δ*hrcC*, which, as expected, did not trigger ion leakage owing to its inability to secrete effectors in the absence of the type III secretion system (Figure 1D,E). Pfo(T3SS) + EV also caused some ion leakage in ME02_01, similarly to Psa3 Δ*33E*, and interestingly this response was also found to be completely abolished by Pfo(T3SS) strains carrying some Psa effectors like *hopF1c*, *hopH1a* and *hopAZ1a* (Figure S3).

2.3 | *A. melanandra* Genome Structure is Orthologous to *A. arguta*

The diploid and Psa-resistant *A. melanandra* (ME02_01 accession) is a more suitable model system than the previously studied tetraploid *A. arguta* AA07_03 (Hemara et al. 2022) for both downstream utility in breeding and functional characterisation of trait genetics. Using Illumina short-read and Oxford Nanopore PromethION long-read platforms, the genome of *A. melanandra* (accession ME02_01) was sequenced and assembled. The genome contained 654.4 Mb from 728 scaffolds with an N50 of ~21.2 Mb (comprising 1746 contigs with N50 ~1.4 Mb), and a Benchmarking Universal Single-Copy Orthologs (BUSCO) score of 98.9%. This assembly is referred to as ME02_01_v2.1 (WGS accession: JBAMMV000000000), from which 637.8 Mb was assigned to 29 chromosomes, aligning Hi-C reads. The gene models from the assembly were used to generate a draft set of 37 047 genes, of which 36 326 (98%) were present on the chromosomes. The final assembly and basic metrics of units (primary, unassigned, gene contents) are provided in Data S1. Phylogenetic analyses of the *Actinidia* species have already shown that *A. arguta* and *A. melanandra* are the closest species among all taxa in the *Actinidia* clade (Tahir et al. 2022). The comparative whole-genome analysis between the publicly available diploid *A. arguta* var. *hypoleuca* (Akagi et al. 2023) and *A. melanandra* genomes show a high conservation of synteny between both species (Figure 2). Notably, the male-specific Y-linked region in *A. melanandra* is also found on chr3 (11.32–11.63 Mb) as in *A. arguta* var. *hypoleuca*, instead of chr25 as in cultivated *A. chinensis* species (Akagi et al. 2023). This is the first comprehensive chromosome-scale genome representing the *A. melanandra* species.

2.4 | The ETI Response of *A. melanandra* to Psa3

To dissect pathways of PTI and ETI in *A. melanandra*, a time-course experiment was performed where axenically grown ME02_01 plants were infiltrated with Psa3 V-13, Psa3 V-13 Δ*hrcC* or buffer alone (mock). Leaf samples were harvested at designated timepoints for RNA extraction and expression analyses (Figure S5). Gene expression (CPM) from all samples and treatments showed no significant differences in counts or quality (Figure S6). Across the full time-series of 0, 3, 6, 10, 20, 30 and 40 h-post infiltration (hpi), a total of 3576 Differentially expressed genes (DEGs) were identified between the Psa3 V-13 treatment versus mock (adjusted $p < 0.001$, |log$_2$ fold-change| > 2). Principal components analysis and a heatmap visualisation of gene expression suggest that there were two subsets of responses: one triggered by Psa3 V-13 and the other by mock and Psa3 V-13 Δ*hrcC* (Figure 3A,B). The early timepoints (3–6 hpi) are crucial for cataloguing PTI responses (expected for both Psa3 V-13 and Psa3 V-13 Δ*hrcC*, but not mock) in common with and diverging from the ETI pathway. Meanwhile, the mid timepoints (10–20 hpi) reflect the threshold time expected for ETI-specific expression, with an ETI response expected for Psa3 V-13 only (Figure S5). Gene expression across the three treatments was clustered into five expression groups. Surprisingly, no gene clusters shared expression between Psa3 V-13 and Psa3 V-13 Δ*hrcC*, even though a strong gene expression response to Psa3 V-13 was observed within four out of five expression clusters, and only Cluster 5 was strongly induced within the Psa3 V-13 Δ*hrcC* treatment (Figure 3A–C).

For Psa3 V-13 treatment, DEGs in Cluster 3 (early Psa3-induced response) peaked earliest at 10 hpi, whereas Cluster 2 DEGs (mid Psa3-induced response) peaked at 20 hpi, with Cluster 1 DEGs (late Psa3-induced response) continuing to increase even at 40 hpi. Cluster 4 (Psa3-suppressed response) and Cluster 5 (Psa3 Δ*hrcC*-induced response) represent a significantly smaller number of DEGs. Unsurprisingly, different subsets of defence-associated phosphorylation-regulating serine-threonine protein kinases were upregulated throughout the responses to Psa3 (Figure 4A–C). Key defence mediator genes, including WRKY transcription factors, mitogen-activated protein kinases, ABC transporters and cytochrome p450s, were abundantly expressed at late timepoints (Figure 4A). Gene families encoding putative E3 ubiquitin ligases, calcium binding proteins, and secretion-associated exocyst components were among the genes upregulated at early to mid-timepoints in response to Psa3 (Figure 4B,C). Various classic defence-response marker genes, including phenylalanine ammonia-lyases (PALs), WRKY and ERF transcription factors, pathogenesis-related proteins, flavin-dependent monooxygenases, and receptor kinase coding genes were upregulated at early to late timepoints specifically in response to Psa3 V-13 (Figure S7). Interestingly, one of the DEGs with the highest level of expression was in Cluster 1 (Figure 4A) and encodes a GRIM-REAPER-like protein which, in *Arabidopsis*, binds to a receptor kinase to trigger ROS-induced cell death (Wrzaczek et al. 2009, 2015). Meanwhile, Psa3 V-13 triggered the suppression of a subset of genes, including RNA recognition and stomatal closure-related proteins (Figure 4D).

Surprisingly, Psa3 V-13 Δ*hrcC* triggered only a weak response using stringent criteria (adjusted $p < 0.001$, |log$_2$ fold-change| > 2) with upregulation of just three genes in Cluster 5, including two defence-associated extension-like proteins (Figure 4E). Excluding DEGs that respond to Psa V-13 and lowering the threshold (adjusted $p < 0.05$) identified only 12
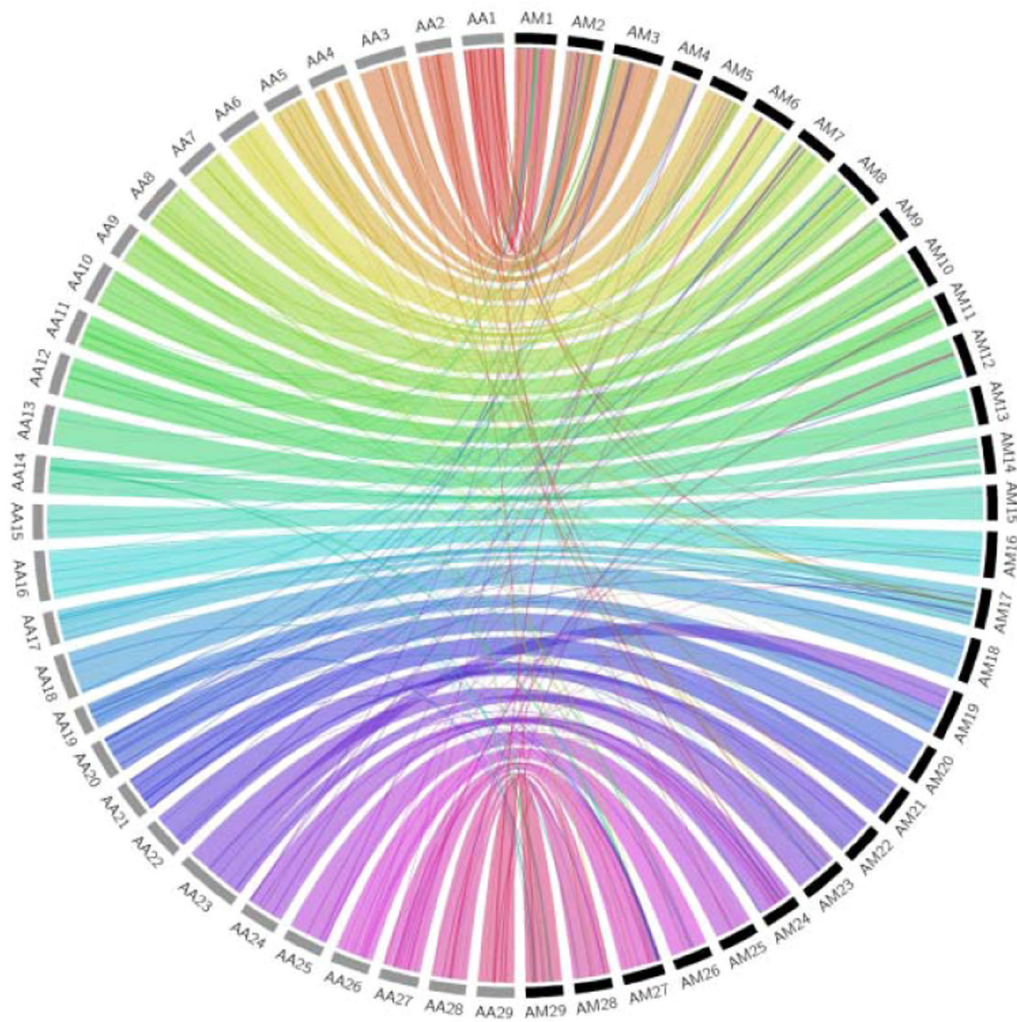
FIGURE 2 | Whole genome (DNA:DNA) synteny Circos plot between chromosomes 1 and 29 from *Actinidia melanandra* ME02_01 (AM) and diploid *Actinidia arguta* var. *hypoleuca* (AA) genome (Akagi et al. 2023). All by all alignments were performed using nucmer as described in the Methods and dnadiff used to filter '1-to-1 coordinates'. Coordinates were converted to Circos links using bundlelinks (−max_gap 1000000 −min_bundle_size 10000). Link bundles were coloured according to chromosome of origin. [Color figure can be viewed at wileyonlinelibrary.com]

DEGs (with high between-replicate variability of expression for these DEGs for the same treatment/time) compared with the mock treatment, suggesting that *A. melanandra* is indeed unable to mount a significant defence response to Psa3 V-13 Δ*hrcC* (Figure S8A,B).

2.5 | Psa3 Δ*33E* and Pfo(T3SS) + *hopA1j* Dependent PTI and ETI Responses in *A. melanandra*

To further characterise *bona fide* ETI and PTI responses in *A. melanandra*, additional bacterial treatments were used in the experimental regime (Figure S5). Sampling for these focused on early (3 and 6 hpi; PTI) and mid (20 hpi; ETI) timepoints, for examining gene expression responses. Gene expression (CPM) from these samples and treatments also showed no significant differences in counts or quality (Figure S9). The three additional treatments included were: Psa3 Δ*33E* (lacking all predicted effectors), Pfo(T3SS) + *hopA1j* (showing ETI in ME02_01, Figure S2), and the non-virulent strain Pfo(T3SS) + EV, and these

were selected for comparison to the previous Psa3 and mock treatments. Psa3 Δ*33E* demonstrates reduced virulence on both *A. chinensis* var. *chinensis* 'Hort16A' and *A. melanandra* ME02_01, similar to Psa3 Δ*hrcC* but does not show reduced in vitro growth or defects in colony morphology (Figure S10). DEGs that are upregulated or downregulated (adjusted $p < 0.001$, |log$_2$ fold-change| > 2) in each bacterial treatment, were filtered out across the three timepoints, from which genes were stacked across timepoints to display the cumulative response profile (Figure 5A–E). Data from Psa3 V-13 and Psa3 V-13 Δ*hrcC* for the same timepoints (used in Figure 3) were also included for comparison. ME02_01 showed a strong transcriptional response to wild-type Psa3 (with 2263 upregulated DEGs and 675 downregulated DEGs) and a significantly mild response to Psa3 V-13 Δ*hrcC* (with 169 upregulated DEGs and 50 downregulated DEGs) (Figure 5A,B). The strong ion-leakage in ME02_01 in response to Pfo(T3SS) + *hopA1j* (Figure S3), was matched with a strong transcriptional response probably due to HopA1j recognition (Figure 5D). A total of 1529 DEGs were upregulated in response to Pfo(T3SS) + *hopA1j* treatment, and 1165 DEGs were downregulated. Consistent with moderate ion-leakage in *A.*
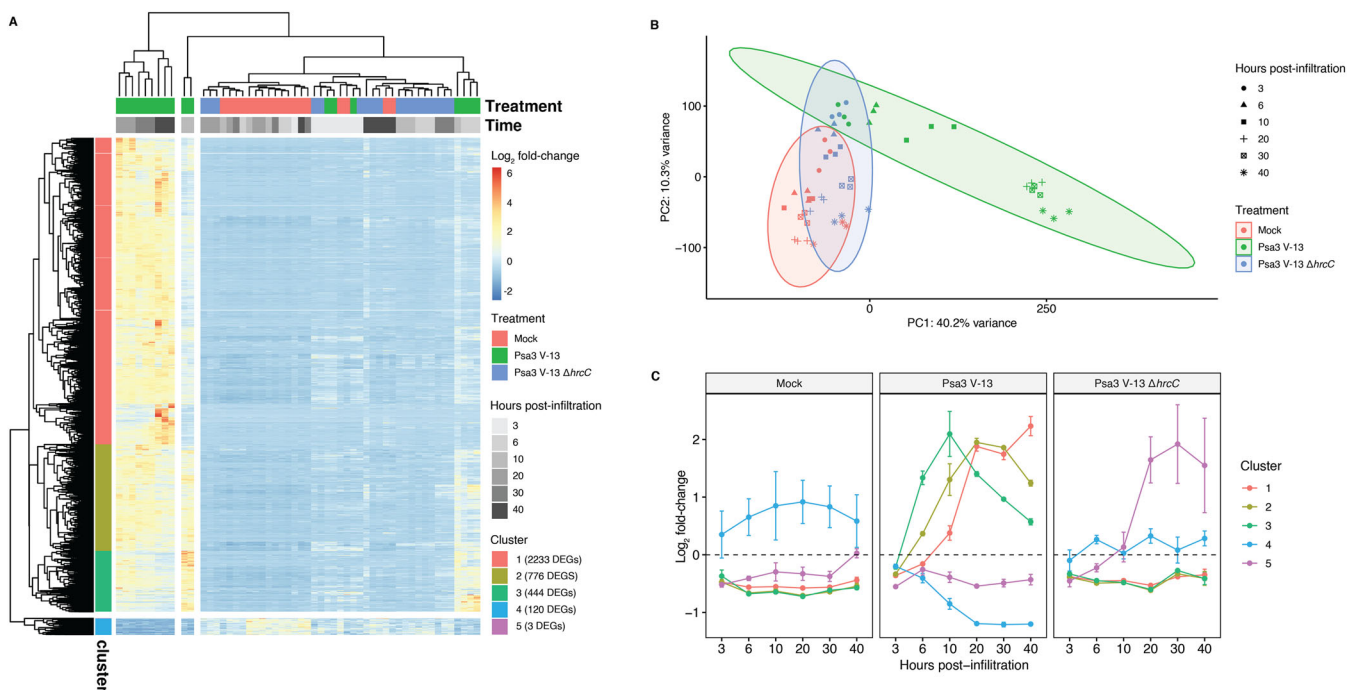
FIGURE 3 | The transcriptional response to *Pseudomonas syringae* pv. *actinidiae* (Psa3) V-13 treatment in *Actinidia melanandra* ME02_01 over time. (A) Heatmap of differentially expressed genes induced by Psa3 V-13 treatment relative to mock (adjusted $p < 0.001$). For each gene, raw counts were transformed by median ratio normalization and Z-score scaling. The pheatmap package was used to generate a heatmap, with genes divided into five hierarchical clusters based on gene expression patterns using the hclust() function. (B) Principal components analysis of gene expression as $\log_2$ fold change for all samples under all treatments and timepoints. (C) Mean $\log_2$ fold-change for each gene expression cluster over the 40-h time series. Error bars indicate standard errors. [Color figure can be viewed at wileyonlinelibrary.com]

melanandra upon Pfo(T3SS) + EV and Psa3 V-13 Δ*33E* treatment (Figures 1D and S3), 1105 DEGs were upregulated and 801 were downregulated in response to Pfo(T3SS) + EV (Figure 5E), and 389 DEGs are upregulated and 449 DEGs are downregulated in response to Psa3 V-13 Δ*33E* compared to the lack of a strong transcriptional response to Psa3 V-13 Δ*hrcC* in *A. melanandra* (Figure 5C). This suggests that *A. melanandra* may be recognising additional components beyond type III secreted effectors in Psa3 V-13 Δ*33E* and Pfo(T3SS) + EV that lack any effectors. These observations are consistent with callose deposition induced by Psa3 V-13, Psa3 Δ*33E*, Pfo(T3SS) + *hopA1j* and Pfo(T3SS) + EV on ME02_01 (Figure 5F,G). Only the Psa3 V-13 Δ*hrcC* and the mock control did not induce callose deposition on ME02_01 (Figure 5G), comparable to the lack of callose deposition in response to Psa3 V-13 treatment of the susceptible *A. chinensis* cultivar 'Hort16A' (Figure 5G).

A heatmap visualisation of *A. melanandra* gene expression for the two early timepoints (3 and 6 hpi) indicates that Pfo(T3SS) + *hopA1j*, Pfo(T3SS) + EV and Psa3 V-13 Δ*33E*, share commonly upregulated genes in Cluster 1 represented by 3922 DEGs (Figure 6A). The mid-timepoint (20 hpi) for Pfo(T3SS) + *hopA1j* shares a similar response in this cluster with Psa3 V-13, indicating that their physiologically independent PTI + ETI responses converge, while PTI-only responses (Psa3 V-13 Δ*33E*, Psa3 V-13 Δ*hrcC* and Pfo(T3SS) + EV) are dampened as quickly and groups with mock-like response in Cluster 2 with 4594 DEGs. Interestingly, the early response by ME02_01 to Psa3 V-13 and Psa3 V-13 Δ*hrcC*, appears to group together with little to no significant genetic response, indicating a lack of a strong

PTI response by *A. melanandra*, supporting the lack of callose deposition seen in response to Psa3 V-13 Δ*hrcC* (Figure 5G). Meanwhile, the strong callose deposition by Psa3 V-13 Δ*33E* and Pfo(T3SS) + EV (Figure 5G) is supported by a strong PTI-like/ non-ETI type transient immune response not shown by Psa3 V-13 Δ*hrcC*, suggesting a recognition of the type III secretion system itself (Figure 6A). Gene ontology term enrichment highlights the different responses to the Psa3 V-13, Psa3 V-13 Δ*33E* and Pfo(T3SS) + EV treatments (Figure S11). While protein phosphorylation and protein kinase activity were upregulated (particularly at 6 hpi) across all treatments, Psa3 V-13 Δ*33E* otherwise only weakly activated a response (Figure S11). Nevertheless, for shared responses of defence-associated phosphorylation, phosphatase activity, vesicle transport and kinase activities, Psa3 V-13 Δ*33E* and Pfo(T3SS) + EV shared early activation (3–6 hpi), with similar responses activated albeit slightly delayed at 6–20 hpi in Psa3 V-13 treatment. The strong non-host response of *A. melanandra* to both Psa3 V-13 and Pfo (T3SS) + EV treatments was enriched for calcium ion binding, vesicle-mediated transport, salicylic acid-mediated signalling, and programmed cell death. In contrast, photosynthesis and transmembrane transport appear to be downregulated in Psa3 V-13 Δ*33E* and Pfo(T3SS) + EV, with the former and not the latter downregulated in response to Psa3 V-13 (Figure S11).

In examining the clusters of gene expression in response to Psa3 V-13 strains in contrast to Pfo(T3SS) strains, a clear segregation of PTI-like genes was seen, exemplified by peroxidases from Cluster 1 that responded transiently to PTI-triggering both strains Pfo(T3SS) and Psa V-13 Δ*33E* but not Psa3 V-13 and Psa3 V-13
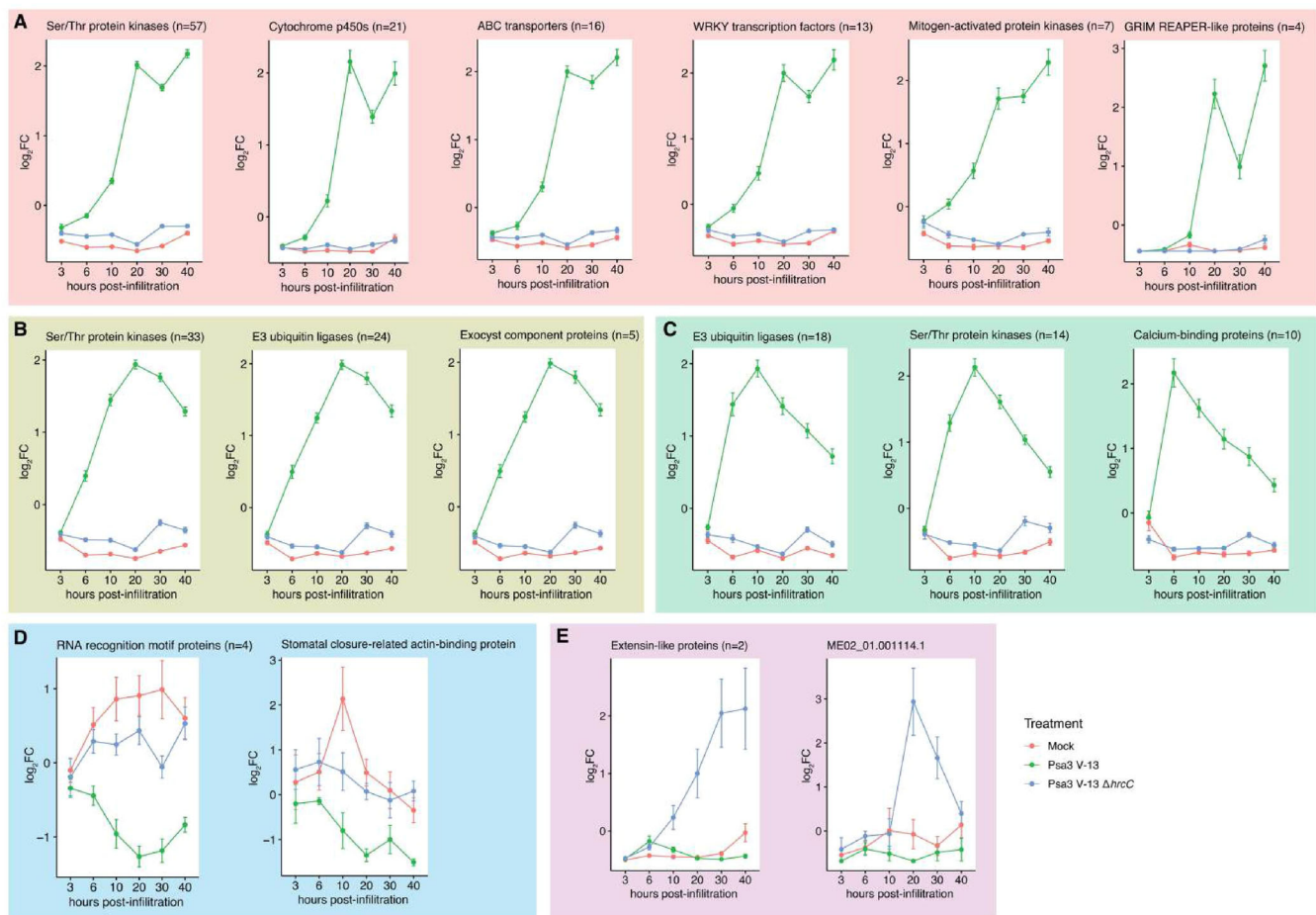
FIGURE 4 | Expression of key families of differentially expressed genes in *Actinidia melanandra* ME02_01 for each treatment and timepoint in (A) early *Pseudomonas syringae* pv. *actinidiae* (Psa3)-induced response Cluster 3, (B) mid-Psa3-induced response Cluster 2, (C) late Psa3-induced response Cluster 1, (D) Psa3-suppressed response Cluster 4 or (E) Psa3 Δ*hrcC*-induced response Cluster 5. Expression for each family is averaged across the number of family members indicated and is plotted as a $\log_2$ fold change for three replicates per sample across indicated timepoints (gene expression of family members passing the significance threshold $p < 0.001$). [Color figure can be viewed at wileyonlinelibrary.com]

Δ*hrcC* (Figure 6B). Similarly, Cluster 3 was represented by protein kinases that are probably activated during PTI (3–6 hpi) but repressed during ETI (Figure 6B). Meanwhile, ETI-associated genes in Cluster 4 responded only to the two ETI-triggering strains at 20 hpi, Psa3 V-13 and Pfo(T3SS) + *hopA1j* (Figure 6B). Cluster 2 represented the largest cluster of genes responsive to Psa3 V-13 treatment, whereby ETI appeared to suppress growth-associated genes, including the auxin-responsive protein family, but surprisingly not affecting Pfo(T3SS) + *hopA1j* and thus this cluster may represent a collection of genes affected by actions of Psa3 V-13 effectors (Figure 6B). Taken together, these results suggest that the innate immune response to Psa3 V-13 (and Pfo (T3SS) + *hopA1j*) is distinct from the somewhat transient immune response seen against other avirulent strains (Psa3 V-13 Δ*33E* and Pfo(T3SS) + EV), none of which is triggered by the T3SS-lacking Psa3 V-13 Δ*hrcC*.

3 | Discussion

This study utilized evidence that effector loss may be selected for in the non-commercial kiwifruit orchards housing Psa-resistant vines to hypothesize a mechanism of resistance to

Psa3. To understand the mechanism of Psa-resistance in one of these Psa-resistant species, *A. melanandra*, transcriptomic analyses of *A. melanandra* in response to wild-type and genetic mutants of Psa3 were undertaken to discover genetic pathways deployed to defend against Psa3 infection. The classic PTI and ETI expression profiles were discovered alongside a surprise that the pattern recognized by *A. melanandra* to trigger PTI constitutes structural components of the T3SS itself.

Psa3 strains that have lost some effectors have been isolated from several *Actinidia* species in the *Actinidia* species germplasm collections in Te Puke, New Zealand, where vines with diverse genotypes are colocated. In this setting, *A. melanandra* and *A. arguta* vines that recognise Psa3 can be located next to vines that do not recognise Psa3 and might not be selected for effector loss. Unsurprisingly, the emergence and spread of effector-loss strains are often limited to specific vines, where related strains can be isolated year after year. Interestingly, the effector-loss strains identified in this study were all obtained from a single block of *A. arguta* 'HortGem'-series cultivars. The effectors lost in this research orchard are unsurprisingly effectors known to be recognized by *A. arguta* (Hemara et al. 2022). In commercial *A. arguta* orchards, vines are always grown in
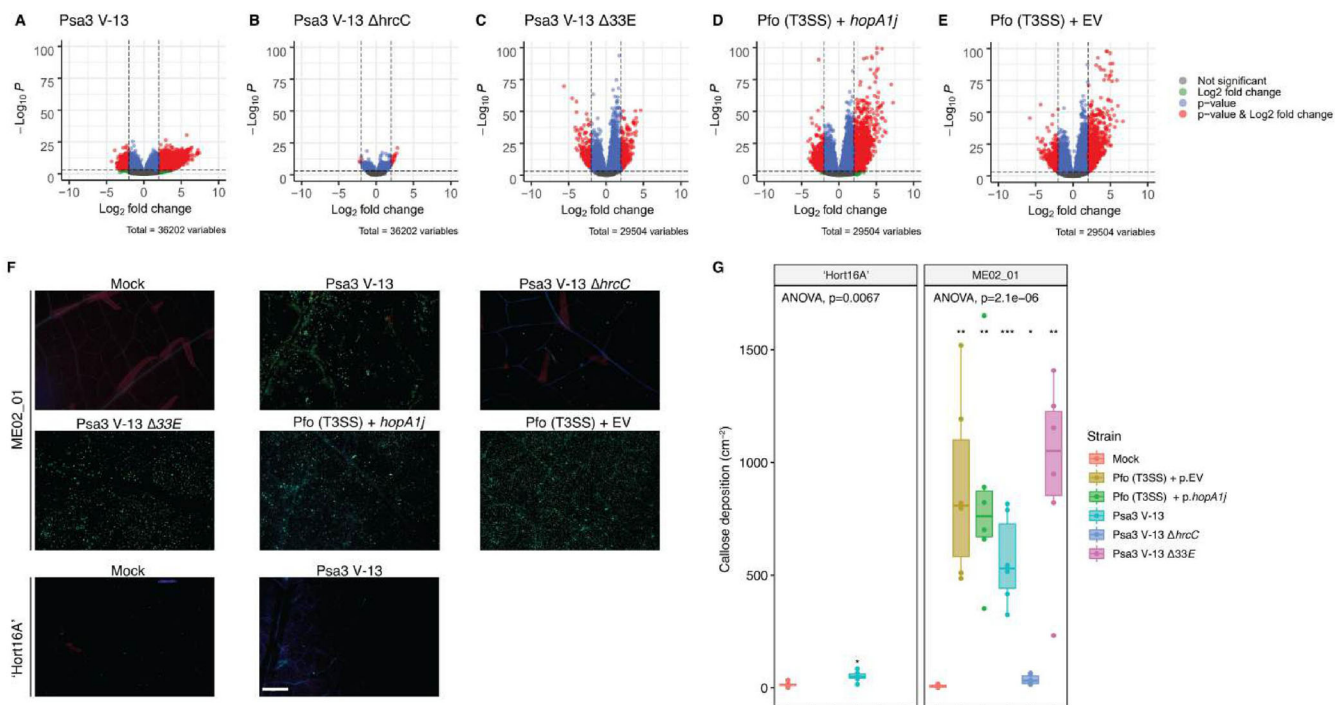
FIGURE 5 | The magnitude of immune response of *Actinidia melanandra* ME02_01 to *Pseudomonas syringae* pv. *actinidiae* (Psa3 strains) or *Pseudomonas fluorescens* (Pfo(T3SS) strains). *A. melanandra* ME02_01 treated with (A) Psa3 V-13, (B) Psa3 V-13 Δ*hrcC*, (C) Psa3 V-13 Δ33*E*, (D) Pfo (T3SS) + *hopA1i* or (E) Pfo(T3SS) + EV. Volcano plots of the differential expressed genes across different treatments (adjusted $p < 0.001$, |$\log_2$ fold-change| > 2). All data are from three biological replicates ($n = 3$) with the 3, 6, 20-h timepoints pooled. (F) Callose deposition induced by Pfo(T3SS) carrying the empty vector (EV) or the positive control *hopA1j*, wild-type Psa3 V-13, Psa3 V-13 Δ*hrcC* or Psa3 V-13 Δ33*E* in *A. melanandra* ME02_01 or *A. chinensis* var. *chinensis* 'Hort16A' leaves. The representative images were captured at 48 h after infiltration with mock (sterile 10 mM MgCl₂) or bacterial strains. (G) The number of callose deposits per cm² of leaf tissue from (F) was analysed with the ImageJ software. Box and whisker plots, with black bars representing the median values from six biological replicates and whiskers representing the 1.5 times interquartile range. Asterisks indicate significant differences from a one-way ANOVA and post hoc Welch's *t*-test between the indicated strain and the mock treatment, where *$p \leq 0.05$, **$p \leq 0.01$, ***$p \leq 0.001$ and ns$p > 0.05$ (not significant). All images were taken under similar conditions and magnification and the scale bar in the final panel represents 500 μm. [Color figure can be viewed at wileyonlinelibrary.com]

monoculture and this may provide more opportunity for these strains to spread and 'sweep' the orchard population. Limited sampling of kiwiberry has been conducted to date (Vanneste et al. 2014; Hemara et al. 2022). However, where an effector-loss strain has emerged in commercial orchards, these strains do not appear to spread across the whole orchard, nor between orchards (Hoyte et al. 2024).

Several studies have delved into the transcriptional response of *Actinidia* genotypes, varying in their susceptibility to Psa3, including immune response markers for ETI and PTI pathways (McAtee et al. 2018; Michelotti et al. 2018; Wang et al. 2018; Song et al. 2019; Nunes da Silva et al. 2022; Qin et al. 2022; Stroud et al. 2022). In a similar vein, transcriptional reprogramming during Psa3-induced ETI in *A. melanandra* involved the expression of canonical marker gene families (Figure S7). These markers of PTI and ETI are well-documented in the scientific literature (Li et al. 2016; Peng, van Wersch and Zhang 2018; Yuan et al. 2021). This is consistent with cumulative evidence in model plants where PTI and ETI have many overlapping subsequent responses, differing predominantly in intensity and progression (Ngou et al. 2021; Yuan et al. 2021). Notably, comparing work on Psa-susceptible *A. chinensis* var. *chinensis* (Michelotti et al. 2018) or *A. chinensis* var. *deliciosa*

(Nunes da Silva et al. 2022), the responses of Psa-resistant *A. arguta* (Nunes da Silva et al. 2022) and *A. melanandra* (Figure S7) appear to be earlier (within 48 hpi) and characterised by a rapid and sustained upregulation of defence genes. This includes upregulated expression of defence hormones and associated transcription factors in response to Psa3, as well as 'late'-acting pathogenesis-related proteins that are typically expressed during ETI under the regulation of the anti-biotroph defence hormone salicylic acid (Michelotti et al. 2018; Nunes da Silva et al. 2022; Stroud et al. 2022).

Meanwhile, the response to PTI-triggering strains was typified by upregulated expression of expected PTI marker genes (Winkelmüller et al. 2021; Hudson et al. 2024). The transcriptomic response to non-virulent effectorless strains Psa3 V-13 Δ33*E* and Pfo(T3SS) + EV intensified between 3 and 6 hpi but waned from 20 hpi, suggesting that the PTI response in *A. melanandra* was transient, consistent with studies from model plants (Figure 6; Li et al. 2016; Bjornson et al. 2021; Winkelmüller et al. 2021). The ETI response in *A. melanandra* was sustained in response to Psa3 V-13 (Figure 6). This same response was mirrored, albeit in a delayed fashion, for Pfo (T3SS) + *hopA1j* (Figure 6). Surprisingly, when compared with Psa3 V-13 and Pfo(T3SS) + *hopA1j* (both expected and observed
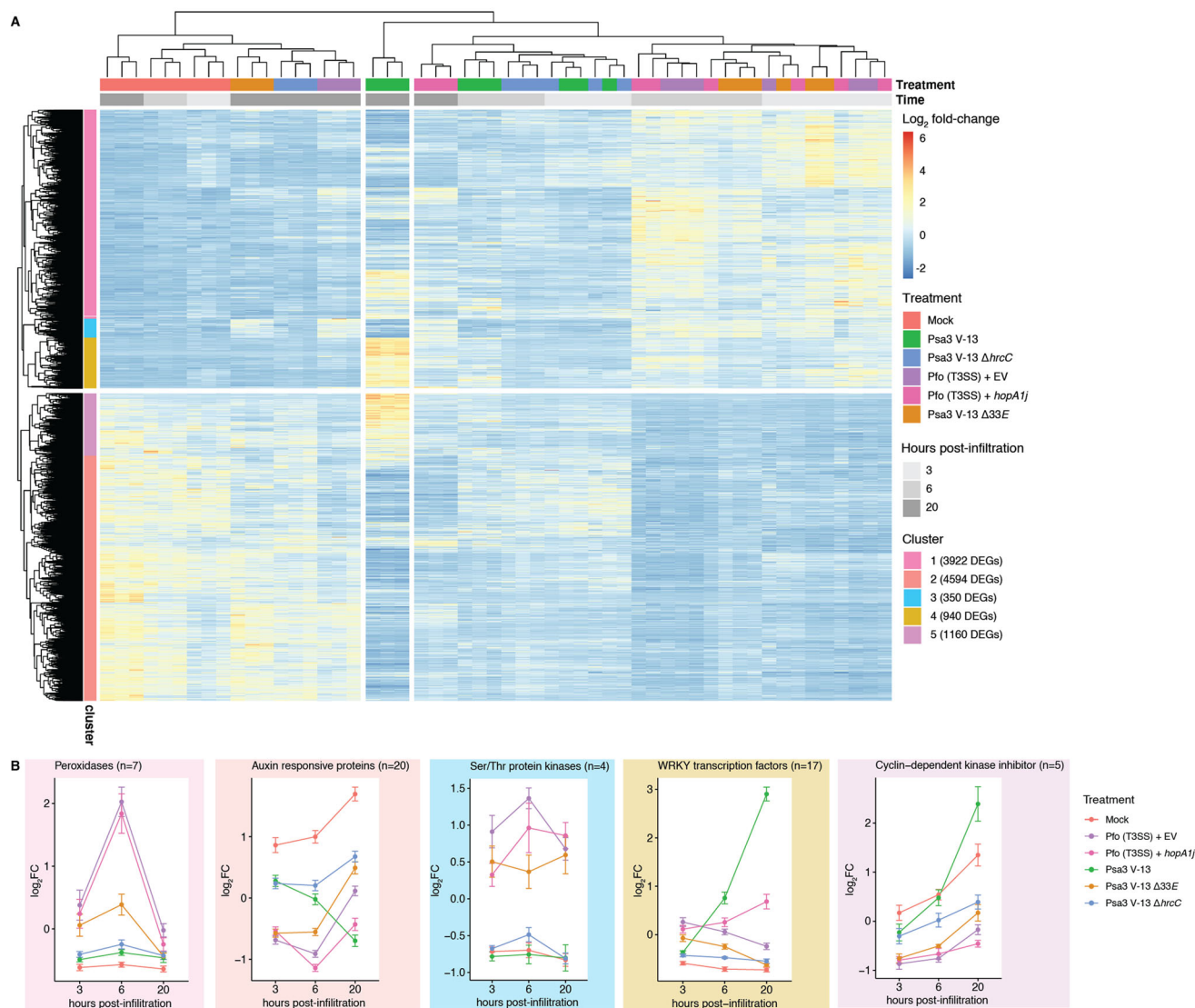
FIGURE 6 | The genetic response of *Actinidia melanandra* ME02_01 is distinct between *Pseudomonas syringae* pv. *actinidiae* (Psa3 strains) and *Pseudomonas fluorescens* (Pfo(T3SS) strains). (A) Heatmap of differentially expressed genes induced by Psa3 V-13, Psa3 V-13 Δ*hrcC*, Psa3 V-13 Δ33E, Pfo(T3SS) + *hopA1i* and Pfo(T3SS) + EV relative to mock (adjusted $p < 0.001$). For each gene, raw counts were transformed by the median of ratios normalization and *Z*-score scaling. The pheatmap package was used to generate a heatmap, with genes divided into five hierarchical clusters based on gene expression patterns using the hclust() function. (B) Expression of key differentially expressed genes by gene cluster in (A) for each treatment and timepoint. Error bars indicate standard errors. [Color figure can be viewed at wileyonlinelibrary.com]

to trigger ETI) or Psa3 V-13 Δ*33E* and Pfo(T3SS) + EV (both expected and observed to trigger PTI), Psa3 V-13 Δ*hrcC* stood out because of a lack of a significant genetic response and reduced intensity of expression (Figures 5 and 6). Similarly, callose deposition, a cell wall fortification response to pathogens, in challenged *A. melanandra* plants was prominent for all expected PTI and PTI + ETI treatments except in Psa3 V-13 Δ*hrcC* (Figure 5F,G). *hrcC*-mutant strains lack a functional T3SS assembly (Roine et al. 1997). This contrast between Psa3 V-13 Δ*hrcC* and Psa3 V-13 Δ*33E*/Pfo(T3SS) + EV suggested that the T3SS itself (or a component of it such as HrcC) is a salient feature in activating PTI in *A. melanandra*. Considering that recognition of Psa3 V-13 Δ*hrcC* response is also absent in 'Hort16A', this suggests a PTI-recognition of the Psa3 T3SS by *Actinidia* spp. may be conserved (Jayaraman et al. 2021). From the kiwifruit breeding perspective, this study demonstrates the

utility of Psa3 effector HopAW1 recognition as well as recognition of the Psa3 T3SS for future mapping of resistance genes in the *A. melanandra* species against Psa3. To our knowledge, this is the first demonstrable opportunity to breed for gene-for-gene resistance in the Psa-kiwifruit pathosystem.

4 | Methodology

4.1 | Kiwifruit Germplasm Survey and Psa3 Isolation

Samples were taken from leaf spots on vines in the *Actinidia* germplasm collections at the Plant & Food Research Te Puke and Kerikeri Research Orchards, as described in Hemara et al. (2022). These two research orchards are located on the North

Island of New Zealand with the Kerikeri Research Orchard (latitude 35.1°) situated more northerly than the Te Puke Research Orchard (latitude −37.8°) but carrying largely similar *Actinidia* genotypes.

Quantitative PCR (qPCR) was carried out on an Illumina Eco Real-Time PCR platform (Illumina), following the protocol outlined by Andersen et al. (2017). Single colonies were tested with Psa-*ITS* F1/R2 PCR primers and primers specific to *hopZ5* to identify Psa3 strains. Samples that amplified in under 30 qPCR cycles were prepared as a 20% (wt/vol) glycerol stock for long-term storage.

4.2 | Psa3 DNA Extraction and Sequencing

Samples collected in 2017 and 2018 were extracted and sequenced as described in Hemara et al. (2022). For samples collected in 2022, DNA was purified using the Wizard Genomic DNA Purification Kit (Promega). Libraries were constructed using the Seqwell Pureplex Unique Dual Index library preparation kit (SeqWell) and were sequenced on an Illumina MiSeq platform (paired-end 150 bp reads) (Illumina).

4.3 | Psa3 Genome Assembly, Variant Calling and Effector Presence Analysis

Quality control reports for the raw sequencing reads were generated using FastQC. Snippy (version 4.6.0) was used to map reads to the reference genome of Psa3 V-13 (CP011972-3) and snippy-core was used to produce a core SNP alignment (Seemann 2015). Gubbins (version 2.4.1) identified recombinant regions in this alignment, producing a filtered alignment of 391 bp (Croucher et al. 2015). RAxML (version 8.2.12; -f a -# 100 −m GTRCAT) was used to generate a maximum-likelihood phylogenetic tree with 100 bootstrap replicates (Stamatakis 2014). The phylogeny and associated metadata were visualised with the R package ggtree (version 2.2.4; Yu et al. 2017). Only bootstrap support values of 50 or above were visualized.

Gene deletions were provisionally identified by CNVnator (version 0.4.1) using snippy's.bam output of reads aligned to the Psa3 V-13 reference (Abyzov et al. 2011). Paired-end reads were assembled using shovill (version 0.9.0) (Seemann 2019). Contigs were annotated with Prokka (version 1.3) (Seemann 2014), preferentially using annotations from the Psa3 V-13 protein model. Pangenome analysis from Roary (version 3.7.0) (Page et al. 2015) identified effector gene presence and absence from the de novo assemblies.

4.4 | Data Visualisation and Statistical Analysis

Statistical analysis was conducted in R (R Core Team 2024), and figures were produced using the packages ggplot2 (Wickham 2016) and ggpubr (Kassambara 2017). Post hoc statistical tests were conducted using the ggpubr (version 0.3.0) and agricolae (version 1.3) packages (de Mendiburu 2017; Kassambara 2017). The stats_compare_means() function from the ggpubr package was used to calculate omnibus one-way analysis of variance (ANOVA) or Kruskal–Wallis statistics to identify statistically significant differences across all treatment groups (Kassambara 2017). For normally distributed populations, Welch's *t*-test was used to conduct pair-wise parametric *t*-tests between an indicated group and a designated reference (Kassambara 2017). For non-normal distributions, a Wilcoxon test was used to conduct pair-wise non-parametric tests between an indicated group and a designated reference (Kassambara 2017). The HSD.test() function from the agricolae package was used to calculate Tukey's honest significant difference (de Mendiburu 2017).

4.5 | Bacterial Strains

Wild-type Psa3 isolates collected from *Actinidia* germplasm are described in Table S1. Psa3 V-13 effector knockout strains used in this study are described in Table S2. Psa3 V-13 Δ*33E* and Pfo (T3SS) plasmid-complemented strains used in this study are described in Table S3.

All Psa3 and Pfo(T3SS) strains were streaked from glycerol stocks onto LB agar supplemented with appropriate antibiotics; plates were sealed and grown for 48 h at 22°C. Overnight shaking cultures were grown in LB supplemented with appropriate antibiotics and incubated at 22°C with 200 rpm shaking. LB agar was supplemented with 12.5 μg/mL nitrofurantoin and 40 μg/mL cephalexin for Psa selection and 20 μg/mL chloramphenicol and 10 μg/mL tetracycline for Pfo(T3SS) selection (all from Sigma-Aldrich). To select for Psa3 and Pfo (T3SS) strains carrying pBBR1MCS-5B vectors, LB agar was supplemented with 25 μg/mL gentamicin (Sigma-Aldrich).

4.6 | Psa3 Complete Effector Knockout

The Psa3 V-13 complete effector knockout strain was generated using the pK18mobsacB-based vectors used previously to generate single knockout strains (Hemara et al. 2022; Jayaraman et al. 2023). The single effectors or effector blocks were sequentially knocked out to generate the 33 effector knockout strain (Psa3 V-13 Δ*33E*) in the order: *hopZ5a/hopH1a* (using the *hopZ5a/hopH1a* double knockout vector), *hopBP1a* (previously *hopZ3*), *hopQ1a*, *hopAS1b*, *avrPto1b* (previously *avrPto5*), *avrRpm1a*, *fEEL* (*avrD1/avrB2b/hopF4a/hopAW1a/hopF1e/hopAF1b/hopD2a/hopF1a*), *hopF1c* (previously *hopF2*), *hopD1a* (using the *hopQ1a/hopD1a* double knockout vector), *CEL* (*hopN1a/hopM1f/avrE1d*), *hopR1b*, *hopAZ1a*, *hopS2b*, *hopY1b*, *hopAM1a-1*, *hopAM1a-2*, *hopBN1a*, *hopW1c* (previously *hopAE1*), *hopAU1a*, *hopI1c* and *hopAH1* block (*hopAG1f/hopAH1c/hopAI1b*). Knockouts were confirmed by PCR and full genome sequencing of the Psa3 V-13 Δ*33E* strain to confirm all effectors were lost. Effectors that did not have a functional type III secretion signal owing to truncation or disruption, or did not possess a HrpL box promoter individually or in an operon (confirmed by expression analysis in McAtee et al. (2018)) were not knocked out and included the following probable pseudogenic effector loci: *avrRpm1c*, *hopA1a*, *hopAA1b*, *hopAT1e* (previously *hopAV1*), *hopAB1b* (previously *hopAY1*). The effectors *hopAA1d* (*CEL* block) and *hopAG1f/hopAI1b* (*hopAH1c* block) were also considered pseudogenes under these criteria,

but were knocked out with other effectors in their block. Effector genes were plasmid-complemented back into Psa3 V-13 $\Delta 33E$ following methodology established in Jayaraman et al. (2020).

4.7 | Callose Deposition Assays

Callose deposit quantification assays were conducted and images acquired as previously described in Jayaraman et al. (2023). Images were analysed using ImageJ software by determining the average area of a single callose deposit and then callose counts calculated based on total callose deposit area in each image.

4.8 | DAB Staining

DAB assay was conducted as described in Jayaraman et al. (2021). Me02-01 leaves, vacuum infiltrated with Psa3 V-13, Psa3 V-13 $\Delta hrcC$ (resuspended in 10 mM MgCl2 and diluted to ~10^8 CFU/mL) and mock (10 mM MgCl$_2$), were harvested and placed on a thin film of water in a sterile tub with lid covered for 48 h. Leaves were then vacuum infiltrated with DAB (3,3′-diaminobenzidine) solution (1 mg/mL DAB in 10 mM Na$_2$HPO$_4$ supplemented with 0.05% Tween 20; all from Sigma-Aldrich). Leaves were incubated in the dark for 6 h and de-stained with chloral hydrate solution (2.5 g per 1 mL water; Merck) for 24–48 h. Leaves were then washed with 70% ethanol and photographed.

4.9 | Pathogenicity Assays

Pathogenicity assays were conducted as described in Hemara et al. (2022). Briefly, *Actinidia* tissue culture plantlets were flooded with Psa inoculum (10^6 CFU/mL). Plantlets were grown in a climate control room at 20°C with a 16 h/8 h light/dark cycle. To quantify bacterial growth *in planta*, leaf disc samples were taken at 0 or 12 dpi.

4.10 | Ion Leakage

Ion leakage was conducted as described in Hemara et al. (2022). Bacterial strains (Table S3) carrying empty vector or effector constructs were streaked from glycerol stocks onto LB agar plates with antibiotic selection, were grown for 2 days at 22°C, and were re-streaked onto fresh agar media, and allowed to grow overnight. Bacteria were then harvested from plates, were resuspended in 10 mM MgCl$_2$, and were diluted to ~10^8 CFU/mL. Leaves were harvested from the tissue culture tubs and were submerged in 30 mL of bacterial inoculum. Vacuum infiltrations were then carried out using a pump and glass bell. For each treatment, leaf discs (6 mm diameter) were harvested from the uniformly vacuum-infiltrated leaf area (6 cm) and were washed in distilled water for 1 h. Six discs were placed in 3 mL of water, and conductivity was measured over 48 h, using a LAQUAtwin EC-33 conductivity metre (Horiba). The standard errors of the means were calculated from five pseudobiological replicates.

4.11 | *A. melanandra* DNA Extraction and Genome Assembly

Leaves of *A. melanandra* (accession ME02_01) were collected from orchard-grown vines at the Plant & Food Research Orchard, Te Puke, New Zealand. The nuclear genomic DNA was extracted with cetyltrimethylammonium bromide-based buffer as described previously (Naim et al. 2012). Hybrid whole genome sequence assembly of ME02_01 was developed using Oxford Nanopore Technologies PromethION data (5 599 455 base-called reads/45.3 Gb data with an estimated coverage of 59.64x) were assembled with Flye (version 2.9.3; Kolmogorov et al. 2019), 10x short-read data (283.00 million reads with an estimated coverage of 52.36x) were assembled with Supernova, 10x Genomics (Weisenfeld et al. 2017) and Hi-C (from Dovetail Genomics, Inc). Independent assemblies from Flye & Supernova were merged using Quickmerge (Chakraborty et al. 2016). Unassigned contigs with 20% or more alignment to existing mitochondrial or chloroplast genome sequences were separated to Fasta subsets containing 46 (mitochondria-related) and 15 (chloroplast-related) contigs. Assembly units were polished with NextPolish (Hu et al. 2020) and placed in linkages groups using aligned Hi-C reads (173.295 million reads mapped in pairs) and the YAHS assembler (version 1.2a.2). The YAHS assembly was critiqued using JuiceBox (Dudchenko et al. 2018). Contigs were placed in linkage groups. The chromosomes were subject to a single round of gap closure using abyss-sealer (Paulino et al. 2015) and Illumina paired-end reads, which closed 8.9% of the gaps. BRAKER3 (Gabriel et al. 2023) was used for gene predictions, along with RNAseq data (in the section below). Chimeric predictions (BRAKER3 prediction, which merged 2 or more separate genes into one prediction) were manually curated in WebApollo2 using physical evidence from RNA-Seq data as well as gene models from closely related *Actinidia* genomes aligned to the genome of ME01_01 using gmap (version 2023-04-28; Wu et al. 2016). The circos plot for the *A. arguta* and *A. melanandra* genomes was developed using Circos (version 0.23-1; Krzywinski et al. 2009) using the alignments performed by nucmer (using '−mum') from MUMmer4 (version 4.0.0; Marçais et al. 2018) with alignment less than 10 kb filtered out.

4.12 | RNAseq and Expression Analyses

The RNAseq experiment was performed on tissue culture-grown plantlets of *A. melanandra* (accession ME02_01), kept at 22°C, 16 h/8 h light/dark cycle. Each tub contained three rooted plants spaced equally. Healthy plants aged between 24 and 36 days were used for the experiment with 8–12 leaves per plant from the top three internodes only. Complete plants were submerged into the respective treatments Psa3 V-13, Psa3 V-13 $\Delta 33E$, Psa3 V-13 $\Delta hrcC$, Pfo(T3SS) + *hopA1j* or Pfo(T3SS) + EV, resuspended in 10 mM MgCl$_2$ at ~10^8 CFU/mL, or mock (10 mM MgCl$_2$) and were vacuum infiltrated into the plants.

For each treatment, nine independent plants in three different tubs were harvested for each timepoint (3, 6, 10, 20, 30 and 40 h), with each biological replicate consisting of leaves from three separate plants. For Psa3 V-13 $\Delta 33E$, Pfo(T3SS) + *hopA1j*, and Pfo(T3SS) + EV, only three timepoints were harvested (3, 6,

20 h). Post-infiltration, only fully infiltrated leaves were harvested and snap-frozen in liquid nitrogen. Leaf tissues without infiltration (untreated) were also harvested just before the infiltration and labelled as 0 h. The full experimental procedure was performed three times, independently. RNA extraction was performed using the Spectrum Plant Total RNA Kit, quantified by spectrophotometry, and equal amounts of the total RNA were pooled up to 3 µg for mRNA short-read sequencing.

High-quality trimmed ($\geq$ Q30) PE (1699.773 million clean reads/572 Gb data) and SE (582.08 million clean reads/58.7 Gb data) mRNA reads (100–150 bp length) were obtained for the samples (10–20 million reads per sample) using DNBSEQ G400 sequencing technology at BGI, Hong Kong, China and Illumina NovaSeq. 6000 sequencing at Australian Genome Research Facility, Melbourne, Australia. The reads were assessed for quality using FastQC (Khetani 2018) and aligned to the reference ME02_01 genome using HiSAT2 (Kim et al. 2019) and sorted BAMs were filtered for high-quality alignments. Feature counts were calculated from the alignments using the subread/1.5.3 package (Liao, Smyth and Shi 2014). For a few gene IDs, where more than one gene models were predicted, the gene ID row with the highest total counts was kept. If there was no significant difference between the alternate splice model, only one representative model was kept.

Differential expression analysis was performed between each bacterial treatment and the mock treatment. DEGs were identified from gene counts using the Bioconductor package DESeq. 2 (version 1.28.0) (Love, Huber and Anders 2014). Principal components analysis of normalised $\log_2$-transformed counts was performed using the estimateSizeFactors(), estimateDispersions() and varianceStabilizingTransformation() functions from DESEQ.2 and the myPCA() function from the R package dataVisEasy. $\log_2$-transformed DEGs with an adjusted $p < 0.001$ were selected for further analysis. Enhanced volcano plots were produced using the lfcshrink() function from DESEQ.2 and the R package EnhancedVolcano (version 1.6.0). Genes with an adjusted $p < 0.001$ and $|\log_2$ fold-change$| \geq 2$ were considered as DEGs. For heatmap and cluster analysis, DEGs with an adjusted p of 0.001 were selected for further analysis irrespective of the magnitude of $\log_2$ fold-change. Heatmaps were generated with the R package pheatmap (version 1.0.12). Raw counts were normalised for heatmap visualisation using custom mor_normalization and cal_z_score functions (https://scienceparkstudygroup.github.io/rna-seq-lesson/06-differential-analysis/index.html). Gene expression and treatment clusters were created by hierarchical clustering using the hclust() function. InterProScan (version 5.59-91.0) was used to provide gene ontology (GO) terms for ME02_01's peptide sequences from the PANTHER, Pfam and CDD databases (Jones et al. 2014). The AgriGO v2 Singular Enrichment Analysis custom analysis tool was used to identify and compare GO term enrichment (Tian et al. 2017).

Conflicts of Interest

The authors declare no conflicts of interest.

Data Availability Statement

The data underlying this article are available in the GenBank Nucleotide Database (https://www.ncbi.nlm.nih.gov/genbank/) and Sequence Read Archive (https://www.ncbi.nlm.nih.gov/sra), including the *Actinidia melanandra* ME02_01 whole genome sequence (JBAMMV000000000) and experimental RNA sequencing reads (PRJNA1080659).

References

Abyzov, A., A. E. Urban, M. Snyder, and M. Gerstein. 2011. "CNVnator: An Approach to Discover, Genotype, and Characterize Typical and Atypical CNVs From Family and Population Genome Sequencing." *Genome Research* 21, no. 6: 974–984. https://doi.org/10.1101/gr.114876.110.

Akagi, T., E. Varkonyi-Gasic, K. Shirasawa, et al. 2023. "Recurrent Neo-Sex Chromosome Evolution in Kiwifruit." *Nature Plants* 9, no. 3: 393–402. https://doi.org/10.1038/s41477-023-01361-9.

Andersen, M. T., M. D. Templeton, J. Rees-George, et al. 2017. "Highly Specific Assays to Detect Isolates of *Pseudomonas syringae* pv. *actinidiae* Biovar 3 and *Pseudomonas syringae* pv. *actinidifoliorum* Directly From Plant Material." *Plant Pathology* 67: 1220–1230. https://doi.org/10.1111/ppa.12817.

Aono, M., T. Miyoshi, H. Yagi, et al. 2024. "Comprehensive Survey of Copper Resistance and Analysis of Responsible Genes in *Pseudomonas syringae* pv. *actinidiae* Biovar 1 and Biovar 3 Isolates From Japan." *Journal of General Plant Pathology* 90, no. 3: 134–143. https://doi.org/10.1007/s10327-024-01169-1.

Bjornson, M., P. Pimprikar, T. Nürnberger, and C. Zipfel. 2021. "The Transcriptional Landscape of *Arabidopsis thaliana* Pattern-Triggered Immunity." *Nature Plants* 7, no. 5: 579–586. https://doi.org/10.1038/s41477-021-00874-5.

Chakraborty, M., J. G. Baldwin-Brown, A. D. Long, and J. J. Emerson. 2016. "Contiguous and Accurate De Novo Assembly of Metazoan Genomes with Modest Long Read Coverage." *Nucleic Acids Research* 44, no. 19: e147. https://doi.org/10.1093/nar/gkw654.

Colombi, E., C. Straub, S. Künzel, M. D. Templeton, H. C. McCann, and P. B. Rainey. 2017. "Evolution of Copper Resistance in the Kiwifruit Pathogen *Pseudomonas syringae* pv. *actinidiae* Through Acquisition of Integrative Conjugative Elements and Plasmids." *Environmental Microbiology* 19, no. 2: 819–832.

Croucher, N. J., A. J. Page, T. R. Connor, et al. 2015. "Rapid Phylogenetic Analysis of Large Samples of Recombinant Bacterial Whole Genome Sequences Using Gubbins." *Nucleic Acids Research* 43, no. 3: e15. https://doi.org/10.1093/nar/gku1196.

Datson, P., S. Nardozza, K. Manako, et al. 2015. "Monitoring the Actinidia Germplasm for Resistance to *Pseudomonas syringae* pv. *actinidiae*." *Acta Horticulturae* 1095: 181–184.

de Mendiburu, F. 2017. agricolae: Statistical Procedures for Agricultural Research [Computer software]. https://CRAN.R-project.org/package=agricolae.

Donati, I., A. Cellini, D. Sangiorgio, et al. 2020. "*Pseudomonas syringae* pv. *actinidiae*: Ecology, Infection Dynamics and Disease Epidemiology." *Microbial Ecology* 80: 81–102.

Dudchenko, O., M. S. Shamim, S. S. Batra, et al. 2018. "The Juicebox Assembly Tools Module Facilitates De Novo Assembly of Mammalian Genomes With Chromosome-Length Scaffolds for Under $1000." *bioRxiv*. https://doi.org/10.1101/254797.

Gabriel, L., T. Brůna, K. J. Hoff, et al. 2024. "BRAKER3: Fully Automated Genome Annotation Using RNA-Seq and Protein Evidence With GeneMark-ETP, AUGUSTUS, and TSEBRA." *Genome Research* 34: 769–777. https://doi.org/10.1101/gr.278090.123.

Hemara, L. M., J. Jayaraman, P. W. Sutherland, et al. 2022. "Effector Loss Drives Adaptation of *Pseudomonas syringae* pv. *actinidiae* Biovar 3 to *Actinidia arguta*." *PLOS Pathogens* 18, no. 5: e1010542. https://doi.org/10.1371/journal.ppat.1010542.

Hoyte, S., J. Jayaraman, L. Hemara, et al. 2024. "Investigating a New Psa Variant in New Zealand." *XI International Symposium on Kiwifruit*.

Hu, J., J. Fan, Z. Sun, and S. Liu. 2020. "NextPolish: A Fast and Efficient Genome Polishing Tool for Long-Read Assembly." *Bioinformatics* 36, no. 7: 2253–2255. https://doi.org/10.1093/bioinformatics/btz891.

Hudson, A., A. Mullens, S. Hind, T. Jamann, and P. Balint-Kurti. 2024. "Natural Variation in the Pattern-Triggered Immunity Response in Plants: Investigations, Implications and Applications." *Molecular Plant Pathology* 25, no. 3: e13445. https://doi.org/10.1111/mpp.13445.

Jayaraman, J., A. Chatterjee, S. Hunter, et al. 2021. "Rapid Methodologies for Assessing *Pseudomonas syringae* pv. *actinidiae* Colonization and Effector-Mediated Hypersensitive Response in Kiwifruit." *Molecular Plant-Microbe Interactions®* 34, no. 8: 880–890. https://doi.org/10.1094/MPMI-02-21-0043-R.

Jayaraman, J., M. Yoon, E. R. Applegate, E. A. Stroud, and M. D. Templeton. 2020. "AvrE1 and HopR1 from *Pseudomonas syringae* pv. *actinidiae* Are Additively Required for Full Virulence on Kiwifruit." *Molecular Plant Pathology* 21, no. 11: 1467–1480.

Jayaraman, J., M. Yoon, L. M. Hemara, et al. 2023. "Contrasting Effector Profiles Between Bacterial Colonisers of Kiwifruit Reveal Redundant Roles Converging on PTI-Suppression and RIN4." *New Phytologist* 238, no. 4: 1605–1619. https://doi.org/10.1111/nph.18848.

Jones, P., D. Binns, H.-Y. Chang, et al. 2014. "InterProScan 5: Genome-Scale Protein Function Classification." *Bioinformatics* 30, no. 9: 1236–1240. https://doi.org/10.1093/bioinformatics/btu031.

Kassambara, A. 2017. ggpubr: "ggplot2" Based Publication Ready Plots [Computer software]. https://CRAN.R-project.org/package=ggpubr.

Khetani, M. P. 2018. Quality Control: Assessing FASTQC Results. Introduction to RNA-Seq Using High-Performance Computing. https://hbctraining.github.io/Intro-to-rnaseq-hpc-salmon/lessons/qc_fastqc_assessment.html.

Kim, D., J. M. Paggi, C. Park, C. Bennett, and S. L. Salzberg. 2019. "Graph-Based Genome Alignment and Genotyping with HISAT2 and HISAT-Genotype." *Nature Biotechnology* 37, no. 8: 907–915. https://doi.org/10.1038/s41587-019-0201-4.

Kolmogorov, M., J. Yuan, Y. Lin, and P. A. Pevzner. 2019. "Assembly of Long, Error-Prone Reads Using Repeat Graphs." *Nature Biotechnology* 37, no. 5: 540–546. https://doi.org/10.1038/s41587-019-0072-8.

Krzywinski, M., J. Schein, İ. Birol, et al. 2009. "Circos: An Information Aesthetic for Comparative Genomics." *Genome Research* 19, no. 9: 1639–1645. https://doi.org/10.1101/gr.092759.109.

Li, B., X. Meng, L. Shan, and P. He. 2016. "Transcriptional Regulation of Pattern-Triggered Immunity in Plants." *Cell Host & Microbe* 19, no. 5: 641–650. https://doi.org/10.1016/j.chom.2016.04.011.

Liao, Y., G. K. Smyth, and W. Shi. 2014. "featureCounts: An Efficient General Purpose Program for Assigning Sequence Reads to Genomic Features." *Bioinformatics* 30, no. 7: 923–930. https://doi.org/10.1093/bioinformatics/btt656.

Liu, Y., D. Li, Q. Zhang, et al. 2017. "Rapid Radiations of Both Kiwifruit Hybrid Lineages and Their Parents Shed Light on a Two-Layer Mode of Species Diversification." *New Phytologist* 215, no. 2: 877–890.

Love, M. I., W. Huber, and S. Anders. 2014. "Moderated Estimation of Fold Change and Dispersion for RNA-Seq Data With DESeq. 2." *Genome Biology* 15, no. 12: 550. https://doi.org/10.1186/s13059-014-0550-8.

Marçais, G., A. L. Delcher, A. M. Phillippy, R. Coston, S. L. Salzberg, and A. Zimin. 2018. "MUMmer4: A Fast and Versatile Genome Alignment System." *PLOS Computational Biology* 14, no. 1: e1005944. https://doi.org/10.1371/journal.pcbi.1005944.

Mauri, S., A. Cellini, G. Buriani, I. Donati, G. Costa, and F. Spinelli. 2016. "Optimization of Cultural Practices to Reduce the Development of *Pseudomonas syringae* pv. *actinidiae*, Causal Agent of the Bacterial Canker of Kiwifruit." *Journal of Berry Research* 6, no. 4: 355–371. https://doi.org/10.3233/JBR-160115.

McAtee, P. A., L. Brian, B. Curran, et al. 2018. "Re-Programming of *Pseudomonas syringae* pv. *actinidiae* Gene Expression during Early Stages of Infection of Kiwifruit." *BMC Genomics* 19, no. 1: 822.

McCann, H. C., L. Li, Y. Liu, et al. 2017. "Origin and Evolution of the Kiwifruit Canker Pandemic." *Genome Biology and Evolution* 9, no. 4: 932–944.

Michelotti, V., A. Lamontanara, G. Buriani, et al. 2018. "Comparative Transcriptome Analysis of the Interaction between *Actinidia chinensis* var. *chinensis* and *Pseudomonas syringae* pv. *actinidiae* in Absence and Presence of Acibenzolar-S-Methyl." *BMC Genomics* 19, no. 1: 585.

Naim, F., K. Nakasugi, R. N. Crowhurst, et al. 2012. "Advanced Engineering of Lipid Metabolism in *Nicotiana benthamiana* Using a Draft Genome and the V2 Viral Silencing-Suppressor Protein." *PLoS One* 7, no. 12: e52717. https://doi.org/10.1371/journal.pone.0052717.

Ngou, B. P. M., H.-K. Ahn, P. Ding, and J. D. G. Jones. 2021. "Mutual Potentiation of Plant Immunity by Cell-Surface and Intracellular Receptors." *Nature* 592: 110–115. https://doi.org/10.1038/s41586-021-03315-7.

Nunes da Silva, M., S. Carvalho, A. M. Rodrigues, A. Gómez-Cadenas, et al. 2022. "Defence-Related Pathways, Phytohormones and Primary Metabolism Are Key Players in Kiwifruit Plant Tolerance to *Pseudomonas syringae* pv. *actinidiae*." *Plant, Cell & Environment* 45, no. 2: 528–541. https://doi.org/10.1111/pce.14224.

Page, A. J., C. A. Cummins, M. Hunt, et al. 2015. "Roary: Rapid Large-Scale Prokaryote Pan Genome Analysis." *Bioinformatics* 31, no. 22: 3691–3693. https://doi.org/10.1093/bioinformatics/btv421.

Paulino, D., R. L. Warren, B. P. Vandervalk, A. Raymond, S. D. Jackman, and I. Birol. 2015. "Sealer: A Scalable Gap-Closing Application for Finishing Draft Genomes." *BMC Bioinformatics* 16, no. 1: 230. https://doi.org/10.1186/s12859-015-0663-4.

Peng, Y., R. van Wersch, and Y. Zhang. 2018. "Convergent and Divergent Signaling in PAMP-Triggered Immunity and Effector-Triggered Immunity." *Molecular Plant-Microbe Interactions®* 31, no. 4: 403–409. https://doi.org/10.1094/MPMI-06-17-0145-CR.

Petriccione, M., L. Zampella, F. Mastrobuoni, and M. Scortichini. 2017. "Occurrence of Copper-Resistant *Pseudomonas syringae* pv. *syringae* Strains Isolated From Rain and Kiwifruit Orchards Also Infected by *P.s.* pv. *actinidiae*." *European Journal of Plant Pathology* 149, no. 4: 953–968.

Poulter, R. T. M., J. Ho, T. Handley, G. Taiaroa, and M. I. Butler. 2018. "Comparison Between Complete Genomes of an Isolate of *Pseudomonas syringae* pv. *actinidiae* From Japan and a New Zealand Isolate of the Pandemic Lineage." *Scientific Reports* 8, no. 1: 10915.

Qin, X., M. Zhang, Q. Li, et al. 2022. "Transcriptional Analysis on Resistant and Susceptible Kiwifruit Genotypes Activating Different Plant-Immunity Processes against *Pseudomonas syringae* pv. *actinidiae*." *International Journal of Molecular Sciences* 23, no. 14: 7643. https://doi.org/10.3390/ijms23147643.

R Core Team. (2024). *R: A Language and Environment for Statistical Computing* [Computer software]. R Foundation for Statistical Computing. https://www.R-project.org/.

Roine, E., W. Wei, J. Yuan, et al. 1997. "Hrp Pilus: An hrp-Dependent Bacterial Surface Appendage Produced by *Pseudomonas syringae* pv. *tomato* DC3000." *Proceedings of the National Academy of Sciences of the United States of America* 94, no. 7: 3459–3464. https://doi.org/10.1073/pnas.94.7.3459.

Scortichini, M., F. Spinelli, and M. D. Templeton. 2023. "The Bacterial Canker of Kiwifruit Caused by *Pseudomonas syringae* pv. *actinidiae*." In *Kiwifruit*, edited by A. Richardson, J. Burdon and R. Ferguson, 317–331. CABI. https://doi.org/10.1079/9781800620933.0018.

Seemann, T. 2014. "Prokka: Rapid Prokaryotic Genome Annotation." *Bioinformatics* 30, no. 14: 2068–2069. https://doi.org/10.1093/bioinformatics/btu153.

Seemann, T. 2015. *snippy: Fast bacterial variant calling from NGS reads* [Computer software]. https://github.com/tseemann/snippy.

Seemann, T. 2019. *Shovill* [Computer software]. https://github.com/tseemann/shovill.

Song, Y., L. Sun, M. Lin, et al. 2019. "Comparative Transcriptome Analysis of Resistant and Susceptible Kiwifruits in Response to *Pseudomonas syringae* pv. *actinidiae* During Early Infection." *PloS One* 14, no. 2: e0211913.

Stamatakis, A. 2014. "RAxML Version 8: A Tool for Phylogenetic Analysis and Post-Analysis of Large Phylogenies." *Bioinformatics* 30, no. 9: 1312–1313. https://doi.org/10.1093/bioinformatics/btu033.

Stroud, E. A., E. H. Rikkerink, J. Jayaraman, and M. D. Templeton. 2022. "Actigard™ Induces a Defence Response to Limit *Pseudomonas syringae* pv. *actinidiae* in *Actinidia chinensis* var. *chinensis* 'Hort16A' Tissue Culture Plants." *Scientia Horticulturae* 295: 110806.

Tahir, J., C. Brendolise, S. Hoyte, et al. 2020. "QTL Mapping for Resistance to Cankers Induced by *Pseudomonas syringae* pv. *actinidiae* (Psa) in a Tetraploid *Actinidia chinensis* Kiwifruit Population." *Pathogens* 9, no. 11: 967. https://doi.org/10.3390/pathogens9110967.

Tahir, J., R. Crowhurst, S. Deroles, et al. 2022. "First Chromosome-Scale Assembly and Deep Floral-Bud Transcriptome of a Male Kiwifruit." *Frontiers in Genetics* 13: 852161. https://doi.org/10.3389/fgene.2022.852161.

Tahir, J., S. Hoyte, H. Bassett, et al. 2019. "Multiple Quantitative Trait Loci Contribute to Resistance to Bacterial Canker Incited by *Pseudomonas syringae* pv. *actinidiae* in Kiwifruit (*Actinidia chinensis*)." *Horticulture Research* 6: 101. https://doi.org/10.1038/s41438-019-0184-9.

Thomas, W. J., C. A. Thireault, J. A. Kimbrel, and J. H. Chang. 2009. "Recombineering and Stable Integration of the *Pseudomonas syringae* pv. *syringae* 61 hrp/hrc Cluster Into the Genome of the Soil Bacterium *Pseudomonas fluorescens* Pf0-1." *Plant Journal* 60, no. 5: 919–928. https://doi.org/10.1111/j.1365-313X.2009.03998.x.

Tian, T., Y. Liu, H. Yan, et al. 2017. "agriGO v2.0: A GO Analysis Toolkit for the Agricultural Community, 2017 Update." *Nucleic Acids Research* 45, no. W1: W122–W129. https://doi.org/10.1093/nar/gkx382.

Vanneste, J. L. 2017. "The Scientific, Economic, and Social Impacts of the New Zealand Outbreak of Bacterial Canker of Kiwifruit (*Pseudomonas syringae* pv. *actinidiae*)." *Annual Review of Phytopathology* 55: 377–399. https://doi.org/10.1079/9781800620933.0018.

Vanneste, J. L., D. A. Cornish, J. Yu, and C. A. Stokes. 2014. "First Report of *Pseudomonas syringae* pv. *actinidiae* the Causal Agent of Bacterial Canker of Kiwifruit on *Actinidia arguta* Vines in New Zealand." *Plant Disease* 98, no. 3: 418.

Wang, T., G. Wang, Z.-H. Jia, D.-L. Pan, J.-Y. Zhang, and Z.-R. Guo. 2018. "Transcriptome Analysis of Kiwifruit in Response to *Pseudomonas syringae* pv. *actinidiae* Infection." *International Journal of Molecular Sciences* 19, no. 2: 373. https://doi.org/10.3390/ijms19020373.

Wang, Z., Y. Liu, L. Li, et al. 2017. "Whole Transcriptome Sequencing of *Pseudomonas syringae* pv. *actinidiae*-Infected Kiwifruit Plants Reveals Species-Specific Interaction Between Long Non-Coding RNA and Coding Genes." *Scientific Reports* 7, no. 1: 4910. https://doi.org/10.1038/s41598-017-05377-y.

Weisenfeld, N. I., V. Kumar, P. Shah, D. M. Church, and D. B. Jaffe. 2017. "Direct Determination of Diploid Genome Sequences." *Genome Research* 27, no. 5: 757–767. https://doi.org/10.1101/gr.214874.116.

Wickham, H. 2016. *ggplot2: Elegant Graphics for Data Analysis*. New York: Springer-Verlag.

Winkelmüller, T. M., F. Entila, S. Anver, et al. 2021. "Gene Expression Evolution in Pattern-Triggered Immunity Within *Arabidopsis thaliana* and Across Brassicaceae Species." *Plant Cell* 33, no. 6: 1863–1887. https://doi.org/10.1093/plcell/koab073.

Wrzaczek, M., M. Brosché, H. Kollist, and J. Kangasjärvi. 2009. "*Arabidopsis* GRI is involved in the Regulation of Cell Death Induced by Extracellular ROS." *Proceedings of the National Academy of Sciences of the United States of America* 106, no. 13: 5412–5417. https://doi.org/10.1073/pnas.0808980106.

Wrzaczek, M., J. P. Vainonen, S. Stael, et al. 2015. "GRIM REAPER Peptide Binds to Receptor Kinase PRK5 to Trigger Cell Death in *Arabidopsis*." *EMBO Journal* 34, no. 1: 55–66. https://doi.org/10.15252/embj.201488582.

Wu, T. D., J. Reeder, M. Lawrence, G. Becker, and M. J. Brauer. 2016. "GMAP and GSNAP for Genomic Sequence Alignment: Enhancements to Speed, Accuracy, and Functionality." In *Statistical Genomics: Methods in Molecular Biology*, edited by E. Mathé and S. Davis, 283–334. New York, NY: Humana Press. https://doi.org/10.1007/978-1-4939-3578-9_15.

Yu, G., D. K. Smith, H. Zhu, Y. Guan, and T. T.-Y. Lam. 2017. "ggtree: An R Package for Visualization and Annotation of Phylogenetic Trees with Their Covariates and Other Associated Data." *Methods in Ecology and Evolution* 8, no. 1: 28–36. https://doi.org/10.1111/2041-210X.12628.

Yuan, M., Z. Jiang, G. Bi, et al. 2021. "Pattern-Recognition Receptors Are Required for NLR-Mediated Plant Immunity." *Nature* 592: 105–109. https://doi.org/10.1038/s41586-021-03316-6.

Supporting Information

Additional supporting information can be found online in the Supporting Information section.